This article has been accepted for publication in IEEE/OSA Journal of Lightwave Technology. This is the author's version which has not been fully edited and content may change prior to final publication. Citation information: DOI 10.1109/JLT.2023.3250438

Revisiting the Stress-Induced Birefringence in Polarization-Maintaining Fibers

Junhao Liu and Tianhua Xu, *Member, IEEE*

***Abstract*—Two conventional errors in the stress-induced birefringence (SIB) of polarization-maintaining fibers (PMFs) are revealed and corrected. The first issue refers to the fundamental expression and its calculation of the SIB, which depends on the selection of stress components. There were obvious inconsistencies in two pioneering reports, while both were widely applied in subsequent works. The second issue is the basic form of the Airy stress function (ASF) in the cross-section plane of the PMF, which dominates the complexity of the stress calculation for SIB. The ASFs in two early pioneering works were different, which led to two different expressions of SIB. Both expressions cannot be reproduced, and calculated results were just around 1/2 of the corresponding measurements. In this paper, both issues have been fixed by revising the definition of SIB and proposing a new ASF form for PMFs. The developed theory is simple and does not have any mathematical contradiction in the calculation process, compare to reported works. Results of the revised SIB based on the developed theory achieve a good agreement with the practical experimental measurements.**

***Index Terms*—Airy stress function, Polarization-maintaining fibers, Principal directions, Principal stresses, Stress components transformation, Stress-induced birefringence.**

I. Introduction

Polarization-maintaining fibers (PMFs) have been widely employed for decades in optical devices such as fiber laser [1], fiber grating [2], fiber interferometer [3], and various fiber sensors [4], especially fiber-optic gyroscopes [5]. The stress-induced birefringence (SIB) which is intrinsic in PMFs is usually very high [6], [7], which enables the fiber to be immune to external perturbations [8], [9]. The SIB critically affects the polarization-maintaining capability of PMFs and hence the performance of systems using PMFs [10], [11]. Generally, the better performance comes from the higher SIB of the fiber, which has already become one of the main targets in the design and fabrication of PMFs [12].

In most PMFs, the SIB is produced through the photo-elastic effect due to the thermal stress from the stress-applying parts (SAPs) embedded in fiber cladding [13], which have different thermal expanding coefficients (TECs) from surroundings due to the dopant [14]. The stress distribution and the SIB depend on the difference between TECs of these constituting materials, which is mainly dominated by the geometry of SAPs in additional to the concentration of the dopant [15], [16]. PMFs were conventionally named Panda, Bow-tie, Elliptical-cladding, and Side-pit fibers, et.al., depending on the geometry of SAPs [6], [7], [13]-[16]. Among them, Panda-PMFs attracted more research interests due to the simple geometry of SAPs, with the same two cylinders symmetrically located at both sides of the core, and are more convenient for the fabrication [12].

In the design, fabrication, and application of PMFs, an analytical formula is required to predict the SIB, although the experimental measurement of the beat length can also provide it via some calculations [8]. Two pioneering works analytically estimated the SIB [13] and the stress distribution [14] based on the Panda-PMFs, in addition to numerical simulations by the finite element method [16]. According to the thermal-elastic displacement potential (TEDP) method from the theory of elasticity, both works developed fundamental models for subsequent research works, and the latter model have been widely applied [17], even in recent works [18].

However, there are two unsolved key technical problems. On one hand, theoretical results from both models [13] and [14] are far smaller than those in the experimental measurements. On the other hand, there are two disagreements in [13] and [14]. Firstly, the selected stress components in calculating the SIB were not consistent with each other, while this was fundamentally related to the definition of the SIB in PMFs, as demonstrated in our recent work for the SIB in Panda-PMFs [15]. Secondly, the expressions of the Airy stress function (ASF) applied in two schemes were not consistent either. Consequently, the reported expressions of the SIB were very complicated and also different in both works, even for the same type of PMFs.

Unfortunately, our previous analyses [15] did not completely solve the above problems, due to the use of the same ASF in the pioneering work [13] and [14]. It caused tedious and contradictory mathematical calculations. Therefore, this pioneering work [14] was only highly cited [17], [18], but has never been fully reproduced. In this paper, both inconsistencies will be comprehensively explained and corrected by revisiting the definition of SIB and proposing a new ASF for Panda-PMFs. The modified definition of SIB in PMFs is clearly presented, which removes the inconsistency in early

This work was supported by EU Horizon 2020 MSCA Grant 101008280 (DIOR) and UK Royal Society Grant (IES\R3\223068). (Corresponding authors: Junhao Liu and Tianhua Xu)

J. Liu is with Tianjin Institute of Electronic Materials, Tianjin 300220, China (e-mail: uceexux@ucl.ac.uk).

T. Xu is with the School of Engineering, University of Warwick, CV4 7AL Coventry, United Kingdom, with Tianjin University, Tianjin 300072, China, and also with University College London (UCL), London WC1E 6BT, United Kingdom (e-mail: tianhua.xu@ieee.org).

This article has been accepted for publication in IEEE/OSA Journal of Lightwave Technology. This is the author's version which has not been fully edited and content may change prior to final publication. Citation information: DOI 10.1109/JLT.2023.3250438

theories. The newly proposed ASF has a very simple form, which introduces a greatly simplified mathematical calculation. Meanwhile, the calculated SIB makes a good agreement with the experimental measurements.

II. THEORY

The two notes on the definition and estimation of the SIB in PMFs are specified and addressed via theoretical analyses in this section.

A. Conventional definition of SIB

According to the Photo-Elasticity, the principal refractive indices n_i ($i=1,2,3$) of materials are related to the principal stresses σ_i ($i=1,2,3$) by [19]:

$$n_1 = n_0 + C_1\sigma_1 + C_2(\sigma_2+\sigma_3), \quad (1)$$

$$n_2 = n_0 + C_1\sigma_2 + C_2(\sigma_3+\sigma_1), \quad (2)$$

$$n_3 = n_0 + C_1\sigma_3 + C_2(\sigma_1+\sigma_2), \quad (3)$$

where C_1 and C_2 are stress-optic constants of the material, respectively.

According to the basic relationship, let the directions of axes in the Cartesian coordinate system describe the projection of the birefringence to the principal directions of the stress field, and thus the "stress birefringence" was defined as [19]

$$\begin{aligned} B &= n_1 - n_2 \\ &= (C_1 - C_2)(\sigma_1 - \sigma_2), \\ &= C\Delta\sigma \end{aligned} \quad (4)$$

where $C = C_1 - C_2$ and $\Delta\sigma = \sigma_1 - \sigma_2$ are the photo-elastic constant and the difference between the principal stresses, respectively.

In fiber optics, the "modal birefringence" of a fiber was defined as [8]

$$B' = n_X - n_Y, \quad (5)$$

where n_X and n_Y are the refractive indices of the slow (denoted by the subscript X from now) and the fast (denoted by the subscript Y from now) axes, respectively.

At the same time, the "modal birefringence" of a fiber was measured as [8]

$$B' = \frac{\lambda}{\Lambda}, \quad (6)$$

where λ and Λ are the wavelength in the free space and the beat length of the fiber, respectively.

For PMFs with the cross-section shown in Fig.1, the "modal birefringence" in (5) equals exactly the "stress birefringence" in (4) induced by the thermal stresses through the photo-elastic effect, as stated in early works [7], [13], [14], [16]. Then the "stress-induced birefringence" (SIB) for PMFs can be written as [15]

$$\begin{aligned} B' &= n_X - n_Y \\ &= (C_1 - C_2)(\sigma_X - \sigma_Y), \\ &= C\Delta\sigma' \end{aligned} \quad (7)$$

where σ_X and σ_Y can be named "normal stresses on axes" (for slow and fast axes, respectively), and $\Delta\sigma'$ is their difference. It will be demonstrated later that these "normal stresses on axes" are different from the principal stresses. That is contrary to the conclusions from pioneering works [13], [14]. For instance, the SIB is 6.2×10^{-4} for a commercial PMF with a 2.5-mm beat length at the 1.55um wavelength. It corresponds to the difference between the normal stresses on the slow and the fast axes of $\Delta\sigma' \approx 1.845\times10^{8}$ Pa under the constant $C = 3.36\times10^{-12}$ /Pa, which is almost twice the value in the reported theory [13] and [14] under the same conditions. This contradiction arises from the relationship between the principal stresses (σ_1, σ_2) in (4) and the "normal stress on axes" (σ_X, σ_Y) in (6). The SIB in PMFs was defined in the Cartesian coordinate system $O(x,y,z)$, but thermal stresses were usually estimated in the polar coordinate system $O(\rho,\theta,z)$. This indicates the reason of the first problem, i.e., the coordinate transformation of stress components for the SIB in PMFs.

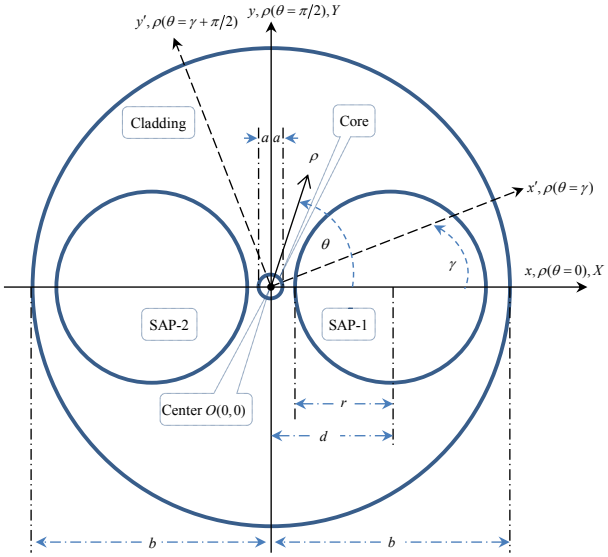

Fig. 1. Two coordinate systems for defining and calculating the SIB of an ideal Panda-PMF, on the cross-section of the fiber with diameters of SAPs $2r$, cladding $2b$, and core $2a$. The polar system with polar radius ρ and angle θ is applied for calculating the stresses and the Cartesian coordinate is employed for defining the SIB. The ideal PMF has a two-fold symmetry about x- and y- axes.

B. Conventional calculation of SIB

As shown in Fig. 1, the polar angle θ in the polar coordinate system starts from the x-axis of the Cartesian (rectangular) coordinate system and goes towards the counter-clockwise as the positive value. The polar angle of a stress point in the polar system also equals the angle of the point in the Cartesian system. The components of stresses at this point in both systems are linked by [20]

$$\sigma_x = \sigma_\rho \cos^2\theta + \sigma_\theta \sin^2\theta - \sigma_{\rho\theta}\sin 2\theta, \quad (8)$$

$$\sigma_y = \sigma_\rho \sin^2\theta + \sigma_\theta \cos^2\theta + \sigma_{\rho\theta}\sin 2\theta, \quad (9)$$

$$\sigma_{xy} = (\sigma_\rho - \sigma_\theta)\sin\theta\cos\theta + \sigma_{\rho\theta}\cos 2\theta, \quad (10)$$

This article has been accepted for publication in IEEE/OSA Journal of Lightwave Technology. This is the author's version which has not been fully edited and content may change prior to final publication. Citation information: DOI 10.1109/JLT.2023.3250438

where $\sigma_{\rho\theta}$ and σ_{xy} are the shear stresses in corresponding systems, respectively. According to the definition in (4), the stress birefringence comes from the difference between the two principal stresses in the Cartesian system, meaning that the shear stress vanishes, i.e., $\sigma_{xy}=0$. Via the basic relationship in (9) we have

$$\tan 2\theta = \pm\frac{2\sigma_{\rho\theta}}{\sigma_{\rho}-\sigma_{\theta}} \tag{11}$$

to represent the principal directions, i.e., the polar angle of principal axes of the birefringence. In the principal directions, the principal stresses are [20]

$$\sigma_1 = \frac{\sigma_x+\sigma_y}{2}+\sqrt{\left(\frac{\sigma_x-\sigma_y}{2}\right)^2+\sigma_{xy}^2}\,, \tag{12}$$

and

$$\sigma_2 = \frac{\sigma_x+\sigma_y}{2}-\sqrt{\left(\frac{\sigma_x-\sigma_y}{2}\right)^2+\sigma_{xy}^2}\,. \tag{13}$$

The directions of the principal stresses, described by angles between the two principal directions and the reference axis, are given by [20]

$$\tan 2\gamma = \pm\frac{\sigma_{xy}}{\sigma_x-\sigma_y}. \tag{14}$$

It is noted that transformation equations in (8) - (10) are valid for stress components at any point expressed in the polar coordinate (ρ,θ) and the Cartesian coordinate (x,y). Then the general formula for calculating the SIB in PMFs by the stresses at an arbitrary point in the polar coordinate (r,θ) is

$$\begin{aligned}\Delta\sigma &= \sigma_1-\sigma_2 = \sqrt{\left(\sigma_x-\sigma_y\right)^2+4\sigma_{xy}^2}\\ &= \sqrt{\left(\sigma_\rho-\sigma_\theta\right)^2+4\left(\sigma_{\rho\theta}\right)^2-2\sigma_{\rho\theta}\left(\sigma_\rho-\sigma_\theta\right)\sin 4\theta}\end{aligned}, \tag{15}$$

and the directions of the two birefringence axes, i.e., their angles to x-axis, are given by (14). Usually it is calculated with one of the four special polar angles for simplicity, such as $\theta=0$, $\pi/2$, $3\pi/2$, and π. Taking the first one $\theta=0$ as an example, the SIB should be

$$\Delta\sigma = \sqrt{\left(\sigma_\rho\big|_{\theta=0}-\sigma_\theta\big|_{\theta=0}\right)^2+4\left(\sigma_{\rho\theta}\big|_{\theta=0}\right)^2}\,. \tag{16}$$

For this case, one of the principal directions determined by (14) is at $\gamma=\theta=0$, which refers to the direction of the slow birefringence axis, i.e., the x-axis of the Cartesian coordinate system in Fig. 1. Meanwhile, the fast birefringence axis, i.e., the other principal direction, is at $\gamma=\theta=\pi/2$ i.e., the y-axis in Fig. 1, according to the theory of elasticity.

From (16) it can be seen that the formula $B=C\left(\sigma_x-\sigma_y\right)$ is not correct, even when we take $\theta=0$ as the x-axis of the Cartesian coordinate system, i.e., $\gamma=0$. We will have

$$\begin{aligned}\sigma_x\big|_{\theta=0} &= \sigma_\rho\big|_{\theta=0}\\ \sigma_y\big|_{\theta=0} &= \sigma_\theta\big|_{\theta=0}\end{aligned}, \tag{17}$$

but there is no evidence for $\sigma_{\rho\theta}\big|_{\theta=0}=0$.

If we wrongly assume that the normal stresses σ_X and σ_Y in (7) are expressed by σ_x in (8) and σ_y in (9), respectively, and take them as the principal stresses σ_1 and σ_2 in (4), respectively, and also wrongly take $B=C\left(\sigma_x-\sigma_y\right)$ like researchers usually did, then the SIB is estimated as

$$\begin{aligned}B &= C\left(\sigma_x-\sigma_y\right)\\ &= C\left[\left(\sigma_\rho-\sigma_\theta\right)\cos 2\theta-2\sigma_{\rho\theta}\sin 2\theta\right]\end{aligned}. \tag{18}$$

This provides exactly the incorrect basic equation (21) in the pioneer work [14], and causes the confusion that the polar angle θ is half the angle of SAPs about the core [17].

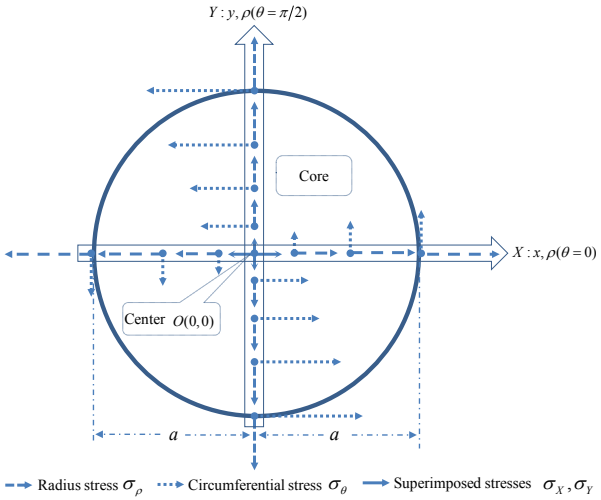

Fig. 2. Schematic of stresses at the points located on the principal axes inside the core. Here we have $\sigma_X>\sigma_Y>0$ for the superimposed stresses, which means a major and a minor tension stresses on the slow and the fast axes, respectively.

C. *Revised SIB in PMFs*

As pointed out in our previous work [15], there are in total four normal stresses contributed to the SIB in PMFs. Two of them come from the conventional principal stresses ($\sigma_\rho\big|_{\theta=0}$ and $\sigma_\theta\big|_{\theta=0}$), the other two refer to their orthogonal counterparts ($\sigma_\rho\big|_{\theta=\pi/2}$ and $\sigma_\theta\big|_{\theta=\pi/2}$). As shown in Fig. 2, there are eight normal stresses (four radial and four circumferential stresses) in the four special directions (positive and negative slow and fast axes, respectively). All components should follow the linear superposition principal.

Considering the symmetry of the stress, $\sigma_\theta\big|_{\theta=\pi/2}=\sigma_\theta\big|_{\theta=\pi/2}$, the normal stresses in the slow and the fast axes can be written as

$$\sigma_X = \sigma_\rho\big|_{\theta=0}+\sigma_\theta\big|_{\theta=\pi/2}, \tag{19}$$

and

$$\sigma_Y = \sigma_\rho\big|_{\theta=\pi/2}+\sigma_\theta\big|_{\theta=0}, \tag{20}$$

This article has been accepted for publication in IEEE/OSA Journal of Lightwave Technology. This is the author's version which has not been fully edited and content may change prior to final publication. Citation information: DOI 10.1109/JLT.2023.3250438

respectively. Then the true SIB in the PMF should be revised as

$$B' = C\left[\left(\sigma_\rho\big|_{\theta=0} + \sigma_\theta\big|_{\theta=\pi/2}\right) - \left(\sigma_\rho\big|_{\theta=\pi/2} + \sigma_\theta\big|_{\theta=0}\right)\right], \quad (21)$$

which arises from the definition of SIB in PMFs as shown in (7). The revised SIB in (21), has the symmetry between the slow and the fast axes, and it can also be rewritten as

$$B' = C\left(\Delta\sigma_X + \Delta\sigma_Y\right), \quad (22)$$

where

$$\Delta\sigma_X = \sigma_\rho\big|_{\theta=0} - \sigma_\theta\big|_{\theta=0}, \quad (23)$$

and

$$\Delta\sigma_Y = -\left(\sigma_\rho\big|_{\theta=\pi/2} - \sigma_\theta\big|_{\theta=\pi/2}\right), \quad (24)$$

should be regarded as the difference between normal stresses experienced in the x-polarization and the y-polarization, respectively.

The revised SIB in PMFs, (21) and (22), can be explained according to the definition of the stress birefringence measurement, where the phase delay between the two linearly polarized light in the two orthogonal directions is measured by the interferometry [19]. Then (21) and (22) are explained in order as follows.

In the extended media such as bulk optical components, which have relatively infinite dimension compared to the wavelength, the phase of a ray is determined by the major principal stress at the points located on the corresponding principal direction. The principal stress (usually the minor one) parallel to the polarization state at the points located on the other (orthogonal) principal direction will not contribute to the phase, since the distance between orthogonal points is sufficiently far compared to the wavelength. On the contrary, in the bounded media such as optical fiber waveguides, the minor principal stress on the other (orthogonal) principal direction will contribute to the phase of the polarized ray in any principal direction. That is to say, the points located on the two principal axes in the fiber core are so close to each other that the paralleled stresses on both axes are linearly superimposed, as described in (19) and (20). This explanation can also be interpreted in another two manners. The first theory treats the linearly polarized light as a series of photons, which are spheres with diameters equal to the wavelength. Each sphere (photon) has three dimensions, which will make it experience both axes in orthogonal directions when it is traveling along the fiber. The other theory supposes that all points on both orthogonal axes are located very close to the central point of the core, i.e., $\rho \to 0$, and then the linear superposition of the stresses from both axes is natural at the central point of the core $\rho = 0$, i.e., the origin point of both coordinate systems.

For the other form of the revised SIB in PMFs according to (22), we can consider that there are two components of the stress differences for SIB, expressed by (23) and (24). One is experienced by the light polarized along the slow axis (x-polarization). The other is experienced by the light polarized along the fast axis (y-polarization). Most of the rays in fibers are helical instead of meridional. It means that most rays in the fiber core will equally experience both components of the revised SIB. The total SIB is the sum of the two components. Here the first negative sign in (24) is to keep the component positive due to the relative variations in magnitudes between the radial and circumferential components.

Figure 3 shows the above process with a flow chart. For simplicity here we used the names of Models I, II, III, and IV, to denote the theories in [13], [14], [15], and the proposed one, respectively. Model IV covers model III as a special scenario by using the same definition of the revised SIB and proposing a new ASF for Panda-PMFs as follows.

D. New ASF for Panda-PMFs

Results in pioneering works [13] and [14] for the Panda-PMF cannot be reproduced in our investigation since there were several mathematical contradictions in [13] and [14]. All these contradictions arise from the forms of the ASF $F(\rho,\theta)$. In order to avoid those contradictions, we propose a new form for the ASF in the Panda-PMF as

$$F(\rho,\theta) = b_0\rho^2 + c_0\rho^2\cos 2\theta, \quad (25)$$

where coefficients b_0, and c_0 are to be determined from the boundary conditions. Following the standard process in [13]-[15], we could get

$$b_0 = \frac{1+v}{1-v}\{\frac{\Delta\alpha_1\Delta T_1}{4}\frac{a^2}{b^2} + \frac{\Delta\alpha_2\Delta T_2 r^2}{4}[\frac{1}{(b-d)^2} + \frac{1}{(b+d)^2} + \frac{2(b^2-d^2)}{(b^2+d^2)^2}]\}, \quad (26)$$

and

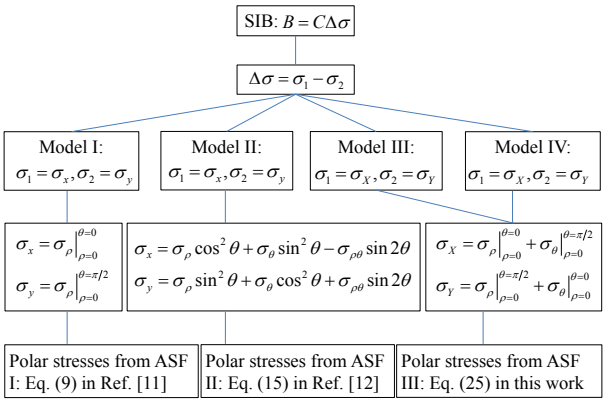

Fig. 3. Block diagram of the mathematical process calculating the SIB in PMFs using previous and proposed models. The SIB is defined by Eq. (4) and the principal indices in Eq. (1)-(3). These principal indices are dominated by the principal stresses in the rectangular coordinate system which defines the SIB. The problem in previous models I and II lies in the transformation of the stresses between the rectangular and the polar coordinate systems since the stresses are calculated in the polar form. One error occurred in the transformation: two stress components were missed in Model I from [13] and the other two stress components were missed in Model II from [14]. Both models led to complicated, inaccurate, and different expressions of SIB, although the same ASF was used. On the contrary, the result based on the corrected definition of SIB from Model III (our previous work [15]) and the new ASF (25) from model IV (our proposed model), is simple and accurate, and contains the previous result in [15] as a special scenario.

This article has been accepted for publication in IEEE/OSA Journal of Lightwave Technology. This is the author's version which has not been fully edited and content may change prior to final publication. Citation information: DOI 10.1109/JLT.2023.3250438

$$c_0=\frac{1+v}{1-v}\{\frac{\Delta\alpha_2\Delta T_2 r^2}{8}[\frac{1}{(b+d)^2}+\frac{1}{(b-d)^2}-\frac{2(b^2-d^2)}{(b^2+d^2)^2}]\}\ . \quad (27)$$

Here r is the radius of SAP, d is the position (distance between its center and the core), and other symbols have same meanings with previous works in [14], [15]. In these calculations all forms of required TEDPs are exactly same as the pioneering [14] and the subsequent works [15], except for the use of the new ASF (25), which results in the coefficients in (26) and (27). It is noted that there is no mathematical contradiction here, compared to the reported work [14], which we cannot reproduce with the same procedures due to some obvious errors in mathematics. This is why we believe the ASF in (25) is feasible, although it is a heuristic form, rather than derived from the theory of elasticity [20].

III. Results

Using the updated (25)-(27), all required stress components can be analytically calculated with low computational complexities. Here we will only focus on stress components in the core area of the PMF, which play the dominant role on the SIB. All intermediate steps in calculations have been skipped since they are exactly the same as in the reported work [14] and our recent work [15]. For simplicity, the following results are calculated based on ideally symmetric Panda-PMFs.

A. Expressions of stresses in core area

The radial stress is given by

$$\begin{aligned}\sigma_\rho\big|_{\rho\le a}=&-\frac{E}{1+v}\{2(b_0-c_0\cos 2\theta)+\frac{1+v}{1-v}\frac{\Delta\alpha_1\Delta T_1}{2}+\frac{1+v}{1-v}\frac{\Delta\alpha_2\Delta T_2}{2}\\&\times[\frac{r^2}{\rho}(\frac{\rho-d\cos\theta}{\rho^2-2\rho d\cos\theta+d^2}+\frac{\rho+d\cos\theta}{\rho^2+2\rho d\cos\theta+d^2})\\&+\frac{r^2}{\rho^2}(-\frac{2(\rho d\sin\theta)^2}{(\rho^2-2\rho d\cos\theta+d^2)^2}+\frac{\rho d\cos\theta}{\rho^2-2\rho d\cos\theta+d^2}\\&-\frac{2(\rho d\sin\theta)^2}{(\rho^2+2\rho d\cos\theta+d^2)^2}-\frac{\rho d\cos\theta}{\rho^2+2\rho d\cos\theta+d^2})]\}\end{aligned} \quad , \quad (28)$$

the shear stress is described as

$$\begin{aligned}\sigma_{\rho\theta}\big|_{\rho\le a}=&\frac{E}{1+v}\{-2c_0\sin 2\theta+\frac{1+v}{1-v}\frac{\Delta\alpha_2\Delta T_2}{2}\frac{r^2}{\rho}\\&\times[\frac{2d\sin\theta}{\rho^2-2\rho d\cos\theta+d^2}-\frac{2\rho d\sin\theta(\rho-d\cos\theta)}{(\rho^2-2\rho d\cos\theta+d^2)^2}\\&-\frac{2d\sin\theta}{\rho^2+2\rho d\cos\theta+d^2}+\frac{2\rho d\sin\theta(\rho+d\cos\theta)}{(\rho^2+2\rho d\cos\theta+d^2)^2}]\}\end{aligned} \quad , \quad (29)$$

and the circumferential stress is expressed as

$$\begin{aligned}\sigma_\theta\big|_{\rho\le a}=&-\frac{E}{1+v}\{2(b_0+c_0\cos 2\theta)+\frac{1+v}{1-v}\frac{\Delta\alpha_1\Delta T_1}{2}-\frac{1+v}{1-v}\frac{\Delta\alpha_2\Delta T_2}{2}\\&\times\frac{r^2}{2}[-\frac{(2\rho-2d\cos\theta)^2}{(\rho^2-2\rho d\cos\theta+d^2)^2}+\frac{2}{\rho^2-2\rho d_2\cos\theta+d_2^2}\\&-\frac{(2\rho+2d\cos\theta)^2}{(\rho^2+2\rho d\cos\theta+d^2)^2}+\frac{2}{\rho^2+2\rho d\cos\theta+d^2}]\}\end{aligned} \quad . \quad (30)$$

All these components depend on the polar radii and angles, besides the material parameters, process parameters, and geometric parameters, which are same as those in early works [13]-[15].

B. Expressions of conventional and revised SIBs

Both conventional SIBs defined in pioneering works [13] and [14] are related to the normal stress components, i.e., the principal stresses, which are all expressed in the polar coordinate system. The normal stresses on the X-direction of the Cartesian coordinate system are

$$\begin{aligned}\sigma_\rho\big|_{\rho\le a}^{\theta=0}=&\sigma_\rho\big|_{\rho\le a}^{\theta=\pi}\\=&-\frac{E}{1-v}\{\frac{\Delta\alpha_1\Delta T_1}{2}(\frac{a^2}{b^2}+1)+\frac{\Delta\alpha_2\Delta T_2 r^2}{4}[\frac{1}{(b-d)^2}+\frac{1}{(b+d)^2}\\&+\frac{6(b^2-d^2)}{(b^2+d^2)^2}+\frac{2}{(\rho-d)^2}+\frac{2}{(\rho+d)^2}]\}\end{aligned} \quad , \quad (31)$$

and

$$\begin{aligned}\sigma_\theta\big|_{\rho\le a}^{\theta=0}=&\sigma_\theta\big|_{\rho\le a}^{\theta=\pi}\\=&-\frac{E}{1-v}\{\frac{\Delta\alpha_1\Delta T_1}{2}(\frac{a^2}{b^2}+1)+\frac{\Delta\alpha_2\Delta T_2 r^2}{4}[\frac{3}{(b-d)^2}+\frac{3}{(b+d)^2}\\&+\frac{2(b^2-d^2)}{(b^2+d^2)^2}-\frac{2}{(\rho-d)^2}-\frac{2}{(\rho+d)^2}]\}\end{aligned} \quad . \quad (32)$$

The normal stresses on the Y-direction are

$$\begin{aligned}\sigma_\rho\big|_{\rho\le a}^{\theta=\pi/2}=&\sigma_\rho\big|_{\rho\le a}^{\theta=3\pi/2}\\=&\frac{-E}{1-v}\{\frac{\Delta\alpha_1\Delta T_1}{2}(\frac{a^2}{b^2}+1)+\frac{\Delta\alpha_2\Delta T_2 r^2}{4}[\frac{3}{(b-d)^2}+\frac{3}{(b+d)^2}\\&+\frac{2(b^2-d^2)}{(b^2+d^2)^2}+\frac{4(\rho^2-d^2)}{(\rho^2+d^2)^2}]\}\end{aligned} \quad , \quad (33)$$

and

$$\begin{aligned}\sigma_\theta\big|_{\rho\le a}^{\theta=\pi/2}=&\sigma_\theta\big|_{\rho\le a}^{\theta=3\pi/2}\\=&\frac{-E}{1-v}\{\frac{\Delta\alpha_1\Delta T_1}{2}(\frac{a^2}{b^2}+1)+\frac{\Delta\alpha_2\Delta T_2 r^2}{4}[\frac{1}{(b-d)^2}+\frac{1}{(b+d)^2}\\&+\frac{6(b^2-d^2)}{(b^2+d^2)^2}-\frac{4(\rho^2-d^2)}{(\rho^2+d^2)^2}]\}\end{aligned} \quad . \quad (34)$$

These equations show that the symmetry about principal axes is automatically satisfied by the stress components using our ASF.

The first conventional SIB defined in the pioneering work [13] is

$$\begin{aligned}B_1=&C\left(\sigma_\rho\big|_{\rho=0}^{\theta=0}-\sigma_\rho\big|_{\rho=0}^{\theta=\pi/2}\right)\\=&\frac{CE}{1-v}\frac{\Delta\alpha_2\Delta T_2 r^2}{2}[\frac{1}{(b-d)^2}+\frac{1}{(b+d)^2}-\frac{2(b^2-d^2)}{(b^2+d^2)^2}]\end{aligned} \quad . \quad (35)$$

The second conventional SIB in the pioneering work [14] is

This article has been accepted for publication in IEEE/OSA Journal of Lightwave Technology. This is the author's version which has not been fully edited and content may change prior to final publication. Citation information: DOI 10.1109/JLT.2023.3250438

$$B_2 = C\left(\sigma_\rho\big|_{\rho\le a}^{\theta=0} - \sigma_\theta\big|_{\rho\le a}^{\theta=0}\right)$$
$$= \frac{CE}{1-v}\frac{\Delta\alpha_2\Delta T_2 r^2}{2}\left[\frac{1}{(b-d)^2}+\frac{1}{(b+d)^2}-\frac{2(b^2-d^2)}{(b^2+d^2)^2}-\frac{2}{(\rho-d)^2}-\frac{2}{(\rho+d)^2}\right] \quad (36)$$

The newly updated SIB [15] is

$$B' = C\left[\left(\sigma_\rho\big|_{\rho\le a}^{\theta=0}+\sigma_\theta\big|_{\rho\le a}^{\theta=\pi/2}\right)-\left(\sigma_\rho\big|_{\rho\le a}^{\theta=\pi/2}+\sigma_\theta\big|_{\rho\le a}^{\theta=0}\right)\right]$$
$$= \frac{CE}{1-v}\Delta\alpha_2\Delta T_2 r^2\left[\begin{array}{l}\dfrac{1}{(b-d)^2}+\dfrac{1}{(b+d)^2}-\dfrac{2(b^2-d^2)}{(b^2+d^2)^2}-\\ \dfrac{1}{(\rho-d)^2}-\dfrac{1}{(\rho+d)^2}+\dfrac{2(\rho^2-d^2)}{(\rho^2+d^2)^2}\end{array}\right]. \quad (37)$$

It can be seen that the revised SIB in (37) has the better symmetry than the conventional models in (35) and (36). Obviously, we have $B'\equiv 0$ for two extreme cases: $r=0$ (no SAPs) and $d=0$ (SAPs are located at the center of the fiber), respectively.

To analyze a more general case of $d\ge a$ and $r\ne 0$, we rewrite (37) as

$$B' = \frac{CE}{1-v}\Delta\alpha_2\Delta T_2 r^2\left(P-Q\right), \quad (38)$$

where

$$P = \frac{1}{(b-d)^2}+\frac{1}{(b+d)^2}-\frac{2(b^2-d^2)}{(b^2+d^2)^2}, \quad (39)$$

and

$$Q = \frac{1}{(\rho-d)^2}+\frac{1}{(\rho+d)^2}-\frac{2(\rho^2-d^2)}{(\rho^2+d^2)^2}, \quad (40)$$

have exactly the same form.

We will have $Q=4/d^2$ when $\rho=0$, i.e., at the center of the fiber core, and the approximation of the revised SIB will lead to an expression of

$$B' = \frac{CE}{1-v}\frac{\Delta\alpha_2\Delta T_2 r^2}{2}\left[\frac{1}{(b-d)^2}+\frac{1}{(b+d)^2}-\frac{2(b^2-d^2)}{(b^2+d^2)^2}-\frac{4}{d^2}\right], \quad (41)$$

which is much simpler than the accurate expression in (37). It is also accurate due to the constant stresses across the core. This will be demonstrated in the next section.

Since $P\ll Q$ in real PMFs, the accurate expression of the revised SIB in (41) could be further approximated as

$$B' = \frac{CE}{1-v}\Delta\alpha_2\Delta T_2 r^2\left(P-Q\right)\approx\frac{-4CE}{1-v}\frac{\Delta\alpha_2\Delta T_2}{2}\left(\frac{r}{d}\right)^2, \quad (42)$$

which is exactly the approximated expression of our previous result [15].

IV. Calculations

In this section we will verify the revised model by numerically calculating the corresponding stresses and their differences. We will focus on the stresses in the core area of

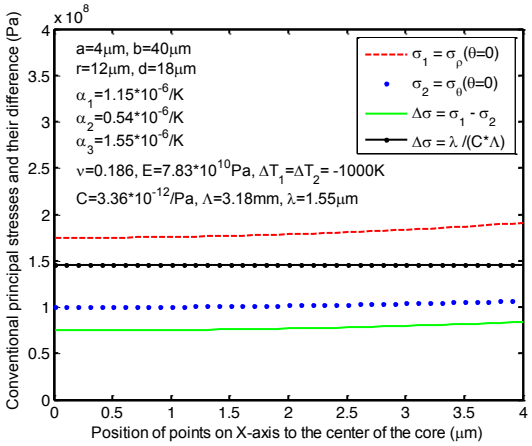

Fig. 4. Two conventional principal stresses (dash and dot) and their difference (solid) inside the fiber core from early models. The theoretical difference for SIB is around 80-MPa for applied parameters. The corresponding SIB is nearly half of that calculated value (145-MPa) from the measured 3.18-mm beat length for modern commercial PMFs (dotted solid).

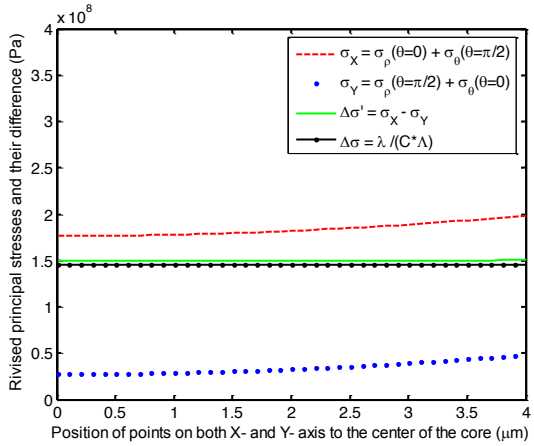

Fig. 5. Two revised principal stresses (dash and dot) and their difference (solid) inside the fiber core with the same parameters as in Fig. 4. The theoretical difference for SIB is around 150-MPa, which is nearly twice the conventionally calculated one and agrees well with the calculated value of 145-MPa from the experimental measurements (dotted solid).

Panda-PMFs required for the calculation of SIB. These calculations used the Panda-PMF with parameters listed in Fig. 4. Geometrical and material parameters are carefully chosen due to their influences on results, based on early research works [12]-[16].

Figure 4 directly shows the principal stresses and their difference in the core area required for the calculation of conventional SIB from the early model [14]. As mentioned before, the stress difference is at the level of 80 MPa, which is nearly half of that calculated from the measured beat length at 3.18-mm for commercial PMFs. This problem was neglected in early models since the values of material parameters were somehow arbitrary, and the stresses and hence the SIB were not very high. Nowadays the 300-MPa stresses for the SIB in a PMF with the beat length of 1.55-mm cannot be practically achieved under the reasonable geometric and material parameters, due to limitations in the fabrication. This indicates that the early model is not very accurate.

This article has been accepted for publication in IEEE/OSA Journal of Lightwave Technology. This is the author's version which has not been fully edited and content may change prior to final publication. Citation information: DOI 10.1109/JLT.2023.3250438

The updated principal stresses and their difference with the same parameters according to the revised SIB model are shown in Fig. 5. There are three common and three different characteristics in the results shown in Fig. 4 and Fig. 5.

The first common property is that all stresses and their differences are similarly constant across the core except for the center of the core. The second common point is that the first conventional and the revised principal stresses in two models are nearly equal to each other. The third common point is that all stresses and their differences are positive, i.e., the stresses on x - and y - axes of the Cartesian coordinate system in both models are tensions, instead of the tensions in x - axes and the compressions in y - axes explained in [4].

With regards to the differences, the first observation is that the stress difference for the revised SIB is nearly twice of that calculated from the conventional model. It is induced by the second observation, i.e., the second revised principal stress ($\Delta\sigma_Y$) is far smaller than the first revised principal stress ($\Delta\sigma_X$), which leads to a higher SIB than that estimated from the conventional model. The last observation is that the revised principal stress difference is close to some constant, since the two stresses have more similar tendency. It means that the revised SIB is closer to some constant than the conventional SIB across the fiber core.

Figure 6 shows the dependency on the angle between two systems of normal stresses on Cartesian axes and their difference for the revised SIB. The angle between the polar and the Cartesian system, denoted by γ, is expressed with the angle between the rotated x-axis (x'-axis) and the fixed axis $\rho_{\theta=0}$, as shown in Fig. 1. The maxima of the corresponding stress difference and the revised SIB, occur at $\gamma=(m-1)\pi/2$, where $m=1,2,3\ldots$ are natural numbers, as shown in Fig. 5 by stars. The negative maxima mean that the slow and the fast axes were swapped with the increase of the angle γ between two systems. The positive maxima occur at $\gamma=(m-1)\pi$, and negative maxima at $\gamma=(2m-1)\pi/2$, have the same absolute values, which is contrary to the early model [13], [14] and validates the efficacy of our model. The zero difference between the revised principal stresses occurs at the angles of $\gamma=(2m-1)\pi/4$, as shown with circles in Fig. 6. This indicates that the two revised principal stresses are equal to each other at these angles, as shown with the rectangular in Fig. 6.

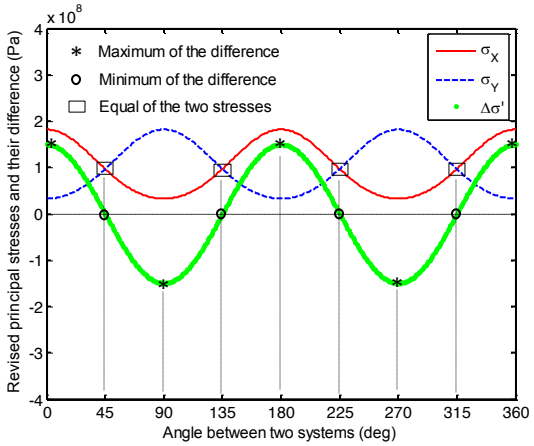

Fig. 6. Dependency on the angle between the polar and the Cartesian systems of revised principal stresses and their difference. The negative differences mean that the two axes are swapped by rotating $(m+1)\pi/2$. Both two principal stresses are positive, indicating that both tension stresses stay in principal directions, rather than one tension in the slow axis and the other compress in the fast axis.

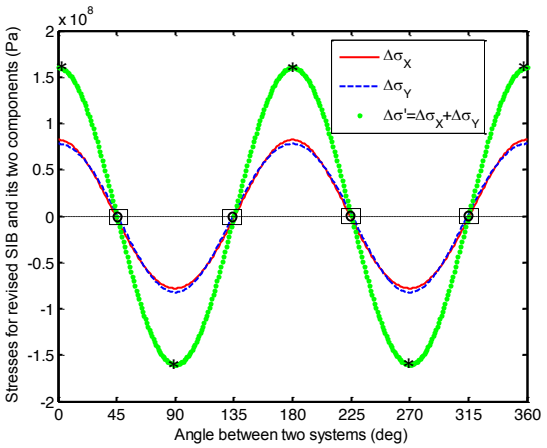

Fig. 7. Dependency of normal stresses on axes of rectangular system and their difference on the angle between the polar and the Cartesian systems, according to the second explanation of the revised SIB. Stresses corresponding to the two components in revised SIB are nearly equal to each other. One of them was missed in the conventional SIB model and this induced the half value of the correct result. The negative values mean the two axes rotated by $(m+1)\pi/2$.

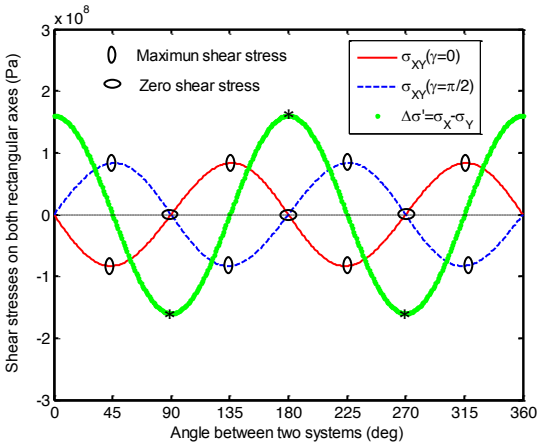

Fig. 8. Dependency of shear stress and principal stresses difference for the revised SIB on axes of rectangular system in the core area. The principal stresses are the normal stresses at the principal directions, where the shear stresses are zero, according to the elasticity theory. The two principal stresses in the two principal directions reflect the maximum and the minimum, respectively, as shown in Fig. 6.

The dependency in Fig. 6 also provides an explanation for the ability of polarization maintaining of PMFs. Only the input light linearly polarized at angles $\gamma=(m-1)\pi/2$ can maintain their linear polarization state during the propagation. The output light will have a linear polarization state similar to the input, which keeps their polarization extinction ratio (PER) close to the input PER in practice, usually over 20-dB. Since

This article has been accepted for publication in IEEE/OSA Journal of Lightwave Technology. This is the author's version which has not been fully edited and content may change prior to final publication. Citation information: DOI 10.1109/JLT.2023.3250438

they will experience the maximum of the revised principal stresses difference, which gives the revised SIB. Those angles refer to the principal axes of the SIB, the x - and y - axes of the rectangular system in Fig. 1, respectively.

The light polarized at angles $\gamma=(2m-1)\pi/4$, i.e., the middle between the two principal axes, cannot maintain their polarization states, which will lead to a PER of 0 dB in the measurements. The light polarized at other angles, will experience the partial polarization-maintaining, and shows a PER between zero and the input polarization state.

Figure 7 shows the two stress differences ($\Delta\sigma_X$ and $\Delta\sigma_Y$) and their sum ($\Delta\sigma'$) using the other explanation of the revised SIB, according to (22). The sum of the two components, i.e., the revised stress difference of SIB, makes a good agreement with Fig. 6. The two components of the normal stress difference in (23) and (24) are very close to each other, which means that they nearly equal each other. However, they are not exactly the same, which indicates the slight difference between the light polarized in the slow and the fast axes. The SIB component is slightly larger on the slow axis than that on the fast axis, according to the revised definition of SIB in PMFs. This may explain the slight difference in the output PER for the light linearly polarized in the slow and the fast axes. The difference between the two components of the revised SIB also explains the inconsistency between the two early models in [13] and [14].

Figure 8 shows the shear stress distribution in the core area. The normal stress differences are also shown for convenient reference. The SIB occurs at the angles where shear stresses are zero, which matches exactly the definition of principal stresses. These angles are the same as the X - and Y - axes in Fig. 1 and Fig. 2, which refer to the principal axes to define the SIB in PMFs via (7).

Figures 8 and 9 show the dependency of the revised principal stresses and their difference on geometric parameters of SAPs, i.e., their positions and radii, respectively. The dependency of stress differences for SIB is similar with reported models [13]-[15]. The stresses and their differences (hence the SIB) increase with the increased radii and decreased positions (their distances to core), respectively. The maximum SIB still occurs at $r=(b-a)/2$ and $d=(b+a)/2$ in theory and is dominated

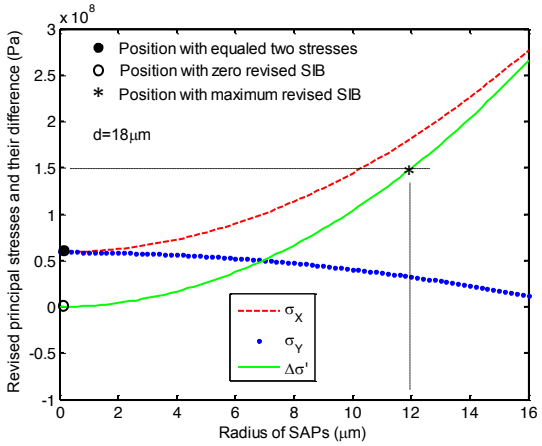

Fig. 10. Dependency of the revised principal stresses inside the core and their difference on the radius of SAPs when their positions are fixed.

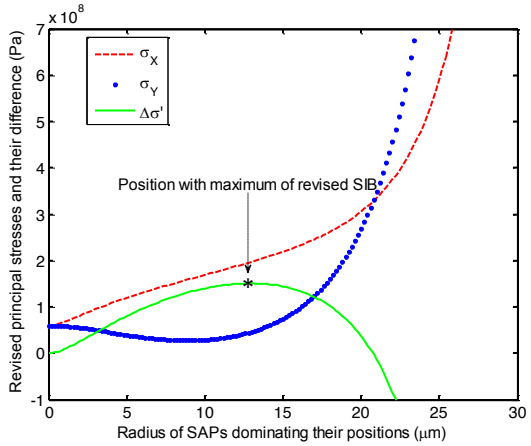

Fig. 11. Dependency of revised principal stresses and their difference on the radii and positions of SAPs from engineering rules.

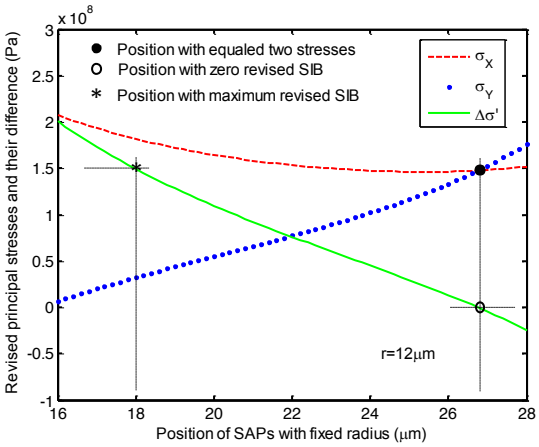

Fig. 9. Dependency of revised principal stresses inside the core and their difference on the positions of SAPs when their radius is fixed.

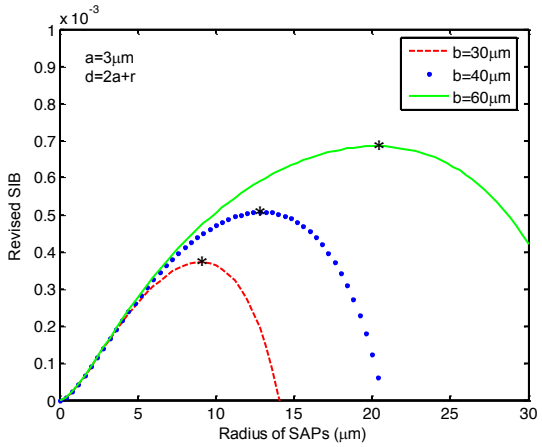

Fig. 12. Dependency of the revised principal stresses and their difference on the radii and positions of SAPs from engineer rules.

This article has been accepted for publication in IEEE/OSA Journal of Lightwave Technology. This is the author's version which has not been fully edited and content may change prior to final publication. Citation information: DOI 10.1109/JLT.2023.3250438

by the material strength [15]. The maximum directly depends on the radii and the distance of SAPs, instead of the subtended angles about the center of the core [17]. The subtended angle depends on the radii and the positions of SAPs, and then the dependency of SIB on them shows the same tendency as in Fig. 9 and Fig. 10.

It is interesting that the two revised principal stresses have the opposite tendencies. For the dependency on the positions of SAPs with fixed radii (Fig. 9), the first revised principal stress is decreasing and the second is increasing. The two principal stresses equal each other at the position where the SIB is zero. As the distance keeps increasing after exceeding that position, the SIB is reversed, i.e., the swap of the slow and the fast axes. It gives the third explanation why the SAPs should not be designed far away from the core, after the first reason for maximizing SIB and the second reason for the mechanical reliability of the fiber [15]. For the dependency on the radii of SAPs with fixed positions (Fig. 10), on the contrary, the first revised principal stress is increasing and the second is decreasing, and the SIB achieves its maximum at the largest radii of SAPs.

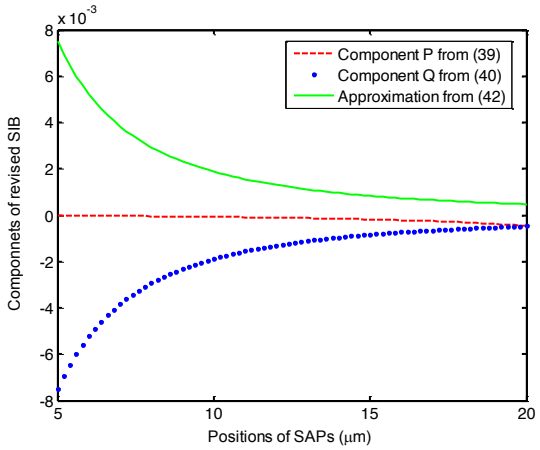

Fig. 13. Dependency of the revised principal stresses inside the core and their difference on the radius of SAPs when their positions are fixed.

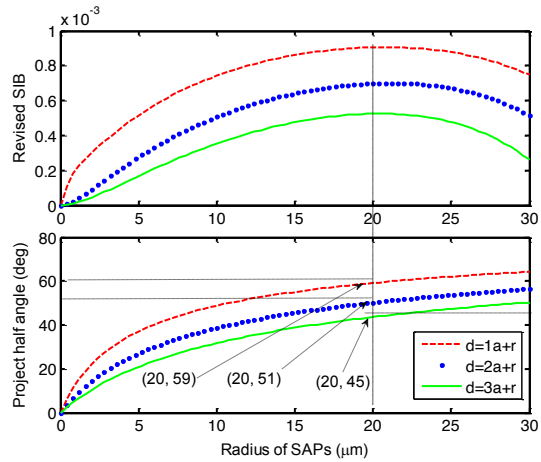

Fig. 14. Dependency of the revised principal stresses inside the core and their difference on the radii of SAPs when their positions are fixed. The occurrence of the maximum SIB at 90° (with half angle 45°) is only valid for the geometry of $d=3a+r$, instead of all types of PMFs. The maximum SIB directly depends on the radius and the distances of SAPs in geometry, which resulted in different angles such as 118° (with half angle 59°) and 102° (with half angle 51°) for $d=a+r$ and $d=2a+r$, respectively.

Figure 11 shows the dependency of revised principal stresses and their difference on the radii and the positions of SAPs in the practical engineering. It is estimated according to the mechanical reliability and the SIB maximization conditions, $r=(b-4a)/2$ and $d=2a+r$, respectively. There will be no physical meanings when the right-hand part with $r>17\mu\text{m}$, according to the mechanical reliability condition.

Figures 9, 10, and 11 also show the design guidelines for geometric parameters of SAPs to maximize the SIB in Panda-PMFs, which are of most interests to the industrial fabrication. According to the basic and the simplified equations in (37) and (41), especially for the approximated one in (42), the SIB depends on the radii (r) and the distances (d) of two SAPs when the material parameters are constant. It shows a simple rule for maximizing the SIB in PMFs, i.e., the SAPs should be larger and closer. There is only one geometric limitation for the guideline, which is that the geometric parameters of SAPs cannot break the configuration of the fiber shown in Fig. 1. This means that we should have $d \geq a$ and $r \leq (b-a)/2$ in theory. Actually, the two "equal" signs will never be achieved in practice considering the optical loss (will dramatically increase at $d=a$) and the mechanical reliability (will dramatically decrease at $d+r=b$). The curves are calculated under the engineering condition $r=(b-4a)/2$ and $d=2a+r$. Under these engineering conditions, the maximum SIB, which is hard to analytically calculate from (42), can be numerically obtained for the design of PMFs. It is achieved at the highest point of the revised principal stress difference in Fig. 11. It also refers to the maximum SIB in the PMFs, as shown in Fig. 12, for three commercial Panda-PMFs with different cladding radii. These marked maxima indicate the optimum design for corresponding PMFs. Figure 13 shows the tendency for different components of the revised SIB in (39) and (40), and the approximated SIB in (42). It verifies the approximated expression since the difference between the two components is so large that the minor one can be neglected.

At last, the role of the projection angle at the core center subtended by one of the SAPs for the early PMF ($2b=125\mu\text{m}$) is shown in Fig. 14. It clarifies the misleading statement that the 90° projection angle is the condition of the SIB maximization [17], which actually is only valid for a particular fiber with $2b=125\mu\text{m}$ and $d=3a+r$, instead of all Panda-PMFs. The SIB only depends on the radii and the positions of SAPs. The projection angle is not explicitly reflected in the revised expression. The sinusoidal value of half of the angle refers to the ratio between the radius and the position. Obviously, the angle depends on the separation between the core and SAPs, i.e., $d-r-a$, which is dominated by the optical loss in the fabrication of the fiber.

V. Conclusion

The definition of the SIB in PMFs has been revisited and modified, and a simple ASF is proposed. Both modifications aim to solve the existing errors in reported well-known models. Compared to early research works where the correct values were halved in the estimation for modern PMFs with high SIB, there are no mathematical contradictions in the proposed model, and the numerically calculated stresses and SIB make good agreements with the practical measurements. This work has pointed out a couple of technical contradictions in well-accepted models and has solved the fundamental legacy issues in the calculation of SIB, and has also provided insightful suggestions for the design and the fabrication of PMFs.

References

1. D. Sun, J. Pei, S. Chu, L. Sun, J. Lu, X. Xu, S. R, "Generation of ultra-high signal to noise ratio harmonics in an all-polarization-maintaining fiber laser," *J. Lightwave Technol.*, vol. 41, no. 1, 01 pp. 255-264, Jan. 2023.
2. A. Anuszkiewicz, M. Bouet, G. Stepniewski, R. Kasztelanic, A. Filipkowski, D. Pysz, A. Cassez, A. Mussot, R. Buczynski, G. Bouwmans, T. Osuch, "Polarization and torsion insensitive fiber Bragg grating written in polarization maintaining ZEBRA fiber with artificial anisotropy," *J. Lightwave Technol.*, vol. 41, no. 2, pp. 726-732, Jan. 2023.
3. Y. Liu, H. Chen, Q. Chen, B. Li, S. Li, "Experimental study on dual-parameter sensing based on cascaded Sagnac interferometers with two PANDA fibers," *J. Lightwave Technol.*, vol. 40, no.9, pp. 3090-3097, Jan. 2022.
4. Z. Fang, K. K. Chin, R. Qu, and H. Cai, *Fundamentals of Optical Fiber Sensors*, John Wiley & Sons, Inc., 2012, Chap.2, Fundamentals of optical fibers, pp. 62.
5. Ha. Li, X. Li, D. Xu, J. Wang, H. Yang, "Improved thermal stability of a fiber optic gyroscope using a geometric birefringence-enhanced polarization-maintaining fiber," *J. Lightwave Technol.*, vol. 42, no. 1, pp. 1-7, Jan. 2023.
6. D. N. Payne, A. J. Barlow, and J. J. R. Hansen, "Development of low- and high-birefringence optical fibers," *IEEE J. Quant. Electron.*, vol. 18, no. 4, pp. 477-487, Apr. 1982.
7. J. Noda, K. Okamoto, and Y. Sasaki, "Polarization-maintaining fibers and their applications", *J. Lightwave Technol*., vol. 4, no. 8, pp. 1071-1085, Aug. 1986.
8. I. P. Kaminow, "Polarization in optical fibers," *IEEE J. Quantum Electron*., vol. 17, no. 1, pp. 15-22, Jan. 1981.
9. S. C. Rashleigh, "Origins and controls of polarization effects in single-mode fibers," *J. Lightwave Technol.*, vol. 1, no. 2, pp. 312-331, Jun. 1983.
10. J. Liu, Y. Liu, and T. Xu, "Bias error and its thermal drift due to fiber birefringence in interferometric fiber-optic gyroscopes," *Opt. Fiber Technol*., vol. 55, no. 102138, Jan. 2020.
11. J. Liu and T. Xu, "Theoretical analysis of the non-reciprocal phase shift due to birefringence and topology in fiber ring interferometers," *Opt. Laser Technol*., vol. 142, no. 107249, May 2021.
12. Y. Sasaki, "Long-length low-loss polarization-maintaining fibers," *J. Lightwave Technol*., vol. 5, no. 9, pp. 1139-1146, Sep. 1987.
13. M. P. Varnham, D.N. Payne, A. J. Barlow, and Robin D. Birch, "Analytic solution for the birefringence produced by thermal stress in polarization-maintaining optical fibers," *J. Lightwave Technol.*, vol. 1, no. 2, pp. 332-339, Jun. 1983.
14. P. L. Chu and R. A. Sammut, "Analytical method for calculation of stresses and material birefringence in polarization-maintaining optical fiber," *J. Lightwave Technol.*, vol. 2, no. 5, pp. 650-662, Oct. 1984.
15. J. Liu Y. Liu, and T. Xu, "Analytical estimation of stress-induced birefringence in Panda-type polarization-maintaining fibers," *IEEE Photon. Technol. Lett*., vol. 32, no. 24, pp. 1507-1510, Dec. 2020.
16. K. Okamoto, T. Hosaka, and T. Edahiro, "Stress analysis of optical fibers by a finite element method," *IEEE Journal of Quant. Electron.*, vol. 17, no. 10, pp. 2123-2133, Oct. 1981.
17. A. Kumar and A. Ghatak, *Polarization of Light with Applications in Optical Fibers*, SPIE Press, 2011, Chap.9, Birefringence in optical fibers: applications, pp.177-179.
18. M. Karimi, F. Surre, T. Sun, K. T. V. Grattan, W. Margulis, and P. Fonjallaz, "Theoretical analysis of a non-symmetric polarization-maintaining single-mode fiber for sensor applications," *J. Lightwave Technol.*, vol. 30, no. 3, pp. 362-367, Feb. 2012.
19. H. Aben and C. Guillemet, *Photoelasticity of Glass*, Springer-Verlag, pp. 56, 1993.
20. S. Timoshenko and J. N. Goodier, *Theory of Elasticity*, 3rd edition, McGraw-Hill Book Company, Inc., 1970, Chap.4, Two-dimensional problems in polar-coordinates, pp. 55-58.

Junhao Liu was born in Yangling, Shaanxi, People's Republic of China in 1980. He received his B.S. degree in Applied Physics from the Northwest University of China, in 2004. Since 2004, he has been as an Engineer with the Division of Fiber-Optic Technology, Tianjin Institute of Electronic Materials, Tianjin, China. His research interests include polarization-maintaining fibers and its application in fiber-optic gyroscopes. He mainly focuses on the stress birefringence, polarization coupling, and mechanical reliability of the fiber. He holds a patent to simply determine the internal rotation of the principal axes in polarization-maintaining fibers.

Tianhua Xu received his PhD degree in School of Information and Communication Technology, at Royal Institute of Technology, Sweden, 2012. His research interests include optical communications, optical sensing, optical networking, as well as machine learn and digital signal processing based compensation of signal distortions. He has published over 120 international journal and conference papers. He has been the technical program committee (TPC) co-chair/member of over 20 IEEE conferences, e.g. GLOBECOM, ICC etc., and the Chair of Optics and Digital Systems Technical Group in Optical Society of America.